

Optimized Enhanced Geothermal Development Strategies with GeoDT and Fracture Caging

Luke P. Frash

Los Alamos National Laboratory, PO Box 1663, Los Alamos, NM 87545

lfrash@lanl.gov

Keywords: EGS, Optimization, Reduced Order Models, Well Spacing, Zonal Isolation, Limited Entry

ABSTRACT

The basis of Enhanced Geothermal Systems (EGS) is the installation of at least one injection well and one production well that are hydraulically connected by engineered flow paths. EGS can be deployed in any hot rock system, including impermeable dry-rock. It is reasonable to expect that an optimized high-efficiency EGS system would be more complex than a simple two-well design. Optimizing EGS developments requires simultaneous consideration of: (1) well layouts, (2) fracture stimulation and flow strategies, (3) three-dimensional fluid flow and heat transfer, (4) injection fluid properties and flow rates, (5) power generation technologies, (6) measurable in-situ properties, (7) induced seismic risk, (8) corrosion and scaling, (9) capital asset utilization factors, and (10) resource assessment. Our recently developed Geothermal Design Tool (GeoDT) brings these factors together in a fast physics-based model to assess the relative effectiveness of various development strategies. We now apply this model with the goal of identifying the key technologies and design needs that could enable safe, sustainable, and efficient EGS development around the globe. Our work predicts optimized well spacing in the 400 m to 700 m range to best utilize in-situ resources while minimizing parasitic losses and seismicity risk. It also sheds light on the need for fracture caging or similar technologies to enable sustained high-rate fluid injection without undue risk of induced seismicity. Due to high variability in fracture permeabilities, limited entry stimulation technology and/or zonal-isolation technologies are shown to be key for efficient power generation.

1. INTRODUCTION

The potential of Enhanced Geothermal Systems (EGS) to provide clean, baseload electrical and thermal energy in the United States and beyond was clearly established by the “Future of Geothermal Energy” report by Massachusetts Institute of Technology (Tester et al., 2006) and the associated predictions have since been revised in the “GeoVision” DOE report (Hamm et al., 2019). This work estimates 60 GWe of attainable geothermal capacity in the United States based on current and foreseeable near-future technologies. Actually achieving this capacity will be a challenge. One of the foremost hurdles to expanding geothermal energy deployment is to overcome its economic risks. The risk stems from: (1) high up front capital costs for resource discovery, evaluation, and validation, (2) uncertainties about subsurface properties that can not be reduced, such as the effect of rock heterogeneity on well stimulation, and (3) the potential for damaging induced seismic events during EGS reservoir creation and operation. Adding to the challenge, these risks arise from complicated multi-physical interactions with geology, engineering design, and socio-economics. In practice, EGS designs that are employed to harvest heat from a geothermal resource have a real potential to cause earthquakes and to under-produce relative to the design targets that are used to justify the expense of capital investments. End-to-end stochastic multi-physics modeling is necessary to confront this challenge.

At the 2021 Stanford Geothermal Workshop, we introduced a new fast geothermal design tool for EGS named GeoDT (Frash, 2021). This tool uses simplified physics to predict fluid flow and heat transfer through 3D networks of fractures and wells. Its base cap abilities include: (1) geothermal reservoir and fracture property prediction, (2) well and fracture placement and meshing, (3) network fluid flow prediction, (4) fracture tensile and shear stimulation, (5) maximum seismic magnitude prediction, (6) long term heat transfer between the fluid and the rock, (7) electrical power output prediction using a Single-flash Rankine Cycle, (8) inputs and outputs structured for machine learning, and (9) data analysis scripts and 3D visualization file outputs. GeoDT completes all of these steps (i.e., 1 to 9) via single threaded code in less than 5 minutes for a 20 year production model with 80 natural fractures and 5 wells using a desktop computer. The numbers in this example do not represent the limits of the code, but larger numbers of fractures and wells require longer times to complete. Dimensions are not mentioned in this example because the code is scale-independent from meters to kilometers size reservoirs. An ARM A conference paper (Frash et al., 2021) gives details on the measurement-based fracture property prediction and scaling theory used in GeoDT. This code is now available open source on GitHub (GeoDesignTool/GeoDT).

The simplified physics are key to achieving GeoDT’s fast code execution times so that more than 10,000 scenarios can be evaluated within hours to days of wall time. With this fast modeling capability, it could become feasible to modify a drilling plan to optimize ultimate productivity while drilling is underway. However, this speed is not without penalty. Here, we rely on reduced-order 1D approximations to estimate fluid flow and heat transfer despite the reality of complex 4D interactions that strongly effect ultimate system performance. Validation of GeoDT is still in progress, but errors in the order of 30% with respect to produced energy would not be surprising. For context, it is important to also point out that heterogeneity and sparse data for the subsurface can cause uncertainties that span multiple orders of magnitude. GeoDT provides a tool to identify the impacts of highly uncertain subsurface conditions on optimized designs for harvesting geothermal heat. By extension, GeoDT provides a means to discover EGS designs and production methods that systematically outperform the alternatives and provides tools to understand why. In this progress update, we present our learnings from applying GeoDT to identify key design parameters that can help to increase the likelihood of success for an EGS project.

In the upcoming results and discussion, we will reference the concept of fracture caging as a key mechanism to improve the performance and predictability of EGS developments. In fracture caging, two or more production wells are drilled to encircle injection wells before hydraulic fracture or hydraulic shear stimulation is performed (Frash et al., 2020). During and after stimulation, these production wells act as a boundary (or cage) for injected fluids to contain the stimulated rock volume and to prevent inadvertent triggering of large seismic events. GeoDT is able to predict the effect of fracture caging to halt new fracture growth, to contain high pressure fluid flow inside leaky fracture networks, and to limit the maximum magnitudes of triggered seismic events. However, this caging approach differs from the accepted conventional EGS development method where microseismic mapping from an initial well stimulation campaign is used to estimate stimulated fracture locations and to subsequently optimally place production wells. In this study, our work predicts that knowledge of the minimum principal stress direction is key to improving the likelihood of successful EGS development but hydraulic stimulation prior to drilling the production wells is not required to achieve success.

2. EXAMPLE EGS MODEL INPUTS AND OUTPUTS

Our analysis starts with assuming no site-specific measurements. This may seem foolish given the greater than 90 inputs that GeoDT requires, however it actually provides an effective basis to demonstrate the value of site-specific data. Here we must point out that reduced uncertainty in a measurable site-specific parameter does not necessarily reduce uncertainty for identifying an optimized EGS design. In this base case, we rely on existing measurements that cover a range of rock types and subsurface situations (Table 1). Water is the working fluid for subsurface flow and power generation via the Rankine steam cycle.

Table 1. Model parameters for a base case scenario having no site-specific measurements

Parameter	Unit	Min.	Nominal	Max.	Deviation	Distribution	Variable	Notes
Domain size (i.e., cubic side length)	m		1500		-	Uniform	size	-
Nominal reservoir depth	m	4000		10000	-	Uniform	ResDepth	Tester et al., 2006
Geothermal gradient	K/km	35		55	-	Uniform	ResGradient	Bearsmore and Cull, 2001
Rock density	kg/m ³	2550		2850	-	Uniform	ResRho	Waples and Waples, 2004
Rock thermal conductivity	W/mK	2.2		2.8	-	Uniform	ResKt	Bearsmore and Cull, 2001
Rock volumetric specific heat capacity	kJ/m ³ K	1850		2150	-	Uniform	ResSv	Waples and Waples, 2004
Ambient surface temperature	C	5		30	-	Uniform	AmbTempC	NOAA
Rock elastic modulus	GPa	50		110	-	Uniform	ResE	Carmichael, 1982
Rock Poisson's ratio	m/m	0.15		0.35	-	Uniform	Resv	Carmichael, 1982
Minimum lateral earth pressure coefficient	Pa/Pa	0.5		0.9	-	Uniform	Ks3	Zoback, 2018
Intermediate earth pressure coefficient	Pa/Pa	0.6		1.2	-	Uniform	Ks2	Zoback, 2018
Fracture set 1 count	fractures	0		40	-	Uniform	fNum	Sub-perpendicular to wells
Fracture set 1 diameter	m	50		1000	-	Uniform	fDia	Sub-perpendicular to wells
Fracture set 1 strike	deg	112		158	-	Uniform	fStr	Sub-perpendicular to wells
Fracture set 1 dip	deg	67		113	-	Uniform	fDip	Sub-perpendicular to wells
Fracture set 2 count	fractures	0		40	-	Uniform	fNum	Sub-parallel to wells
Fracture set 2 diameter	m	50		1000	-	Uniform	fDia	Sub-parallel to wells
Fracture set 2 strike	deg	22		67	-	Uniform	fStr	Sub-parallel to wells
Fracture set 2 dip	deg	67		113	-	Uniform	fDip	Sub-parallel to wells
Fracture set 3 count	fractures	0		40	-	Uniform	fNum	Sub-parallel to wells conjugate set
Fracture set 3 diameter	m	50		1000	-	Uniform	fDia	Sub-parallel to wells conjugate set
Fracture set 3 strike	deg	90		270	-	Uniform	fStr	Sub-parallel to wells conjugate set
Fracture set 3 dip	deg	-22		23	-	Uniform	fDip	Sub-parallel to wells conjugate set
Shear displacement-length coefficient (γ)	m/m	0.001	0.01	0.063	0.01	Trunc. Lognormal	gamma	Frash et al., 2021
Shear displacement-length exponent ($n1$)	-		1		-	Uniform	n1	Frash et al., 2021
Shear displacement-dilation coefficient (a)	m/m	0	0.2	0.8	0.2	Truncated Normal	a	Frash et al., 2021
Shear displacement-dilation exponent (b)	-		1		-	Uniform	b	Frash et al., 2021
Witherspoon factor (N)	m/m	0	0.6	2	0.6	Special	N	Frash et al., 2021
Fracture compressibility (a)	1/MPa	2.00E-9	2.90E-8	1.00E-7	2.90E-8	Truncated Normal	Alpha	Frash et al., 2021
Initial hydraulic aperture (bi)	m	0.00005	0.0005	0.002	0.0005	Truncated Normal	bh	Frash et al., 2021
Boundary hydraulic aperture	m	0.0001		0.002	-	Uniform	bh_bound	-
Fracture roughness	-	0.7		1	-	Uniform	f_roughness	-
Well count	wells	1		6	-	Uniform	w_count	-
Well spacing	m	200		1100	-	Uniform	w_spacing	-
Well length	m	800		1200	-	Lognormal	w_length	-
Well azimuth	deg	0		90	-	Uniform	w_azimuth	-
Well dip	deg	0		90	-	Uniform	w_dip	-
Well proportion	deg	0.4		1	-	Uniform	w_proportion	-
Well phase	deg	0		360	-	Uniform	w_phase	-
Well toe	deg	-15		15	-	Uniform	w_toe	-
Well skew	deg	-15		15	-	Uniform	w_skew	-
Well intervals	zones	1		10	-	Uniform	w_intervals	-
Casing inner radius	m	0.1		0.23	-	Uniform	ra	Oil County Tubular Goods, 2020
Casing outer radius	m		ra +0.013		-	-	rb	-
Borehole radius	m		rb +0.013		-	-	rc	-
Hazen-Williams friction coefficient	-		80		-	-	rgh	Jeppson, 1974
Cement thermal conductivity	W/mK		2		-	-	CemKt	Asadi et al., 2018
Cement volumetric specific heat capacity	kJ/m ³ K	2000			-	-	CemSv	Koduri, 2014
Electrical generator efficiency	%		0.85		-	-	GenEfficien	Electropaedia, 2022
Project lifespan	yr		20.5		-	-	LifeSpan	Vitaller et al., 2020
Power plant inlet pressure	MPa		1		-	-	p_whp	-
Injection temperature	C		95		-	-	Tinj	-
Borehole thermal convection coefficient	kW/m ² K		3		-	-	H_ConvCoef	Kosky et al., 2013
Water density for flow analysis	kg/m ³	980			-	-	PoreRho	Cooper and Dooley, 2007
Water dynamic viscosity	cP		0.25		-	-	Poremu	Huber et al., 2009
Perforation count per injection interval	perfs		1		-	-	perf	-
Production well pressure change from pore	MPa	-10		2	-	Uniform	dPp	-
Stimulation flow rate	m ³ /s	0.02		0.08	-	Uniform	Qstim	Quote for UtahFORGE
Stimulation volume	m ³	9		1700	-	Uniform	Vstim	Quote for UtahFORGE
b-value (Gutenberg Richter)	-		1		-	-	b_value	Gutenberg and Richter, 1956
Fracture friction angle	-	20		55	-	Uniform	phi	Lab shear tests
Fracture cohesion	MPa	0		20	-	Uniform	mcc	Lab shear tests
Circulation injection flow rate	m ³ /s	0.005		0.05	-	Uniform	Qinj	-

* Note: White (no color) signifies parameters that can be measured but not without uncertainty. Blue highlights controllable design parameters. Pink highlights parameters that are challenging or infeasible to measure in-situ. Blank values (-) indicate that no reference is available so a value must be assumed or that no value was needed for the associated parameter.

GeoDT uses more than 80 unique parameters. Many parameters are stochastic, such as those to place and estimate the properties of natural fractures. The intent here is to encourage acceptance that unknown permeable faults and fractures could exist in a site unless measurements show otherwise. Oppositely, known faults and fractures could be relatively impermeable unless proven otherwise. Colors are included in Table 1 to highlight (blue) controllable design parameters, (pink) parameters that are challenging or infeasible to measure in-situ, and (white) parameters that can be measured but not without uncertainty. The user's selection of which parameters are stochastic versus not is a subjective process that depends on the goals of the analysis. For example, we take steam turbine electrical generation efficiency as a constant 0.85 (i.e., 85%) because we do not yet wish to address capital utilization factors and associated inefficiencies in the analysis. Conversely, we do not wish to overly constrain the initial hydraulic aperture of natural fractures (i.e., permeability) since this value is typically unknown, even with excellent site-specific data.

Several statistical distributions are used in this base case. Single values are set for constants. Maximum and minimum values are shown for uniformly distributed values. A nominal (mean) value and standard deviation are provided for normally and log-normally distributed values. Truncated distributions have maximum and minimum values as shown. The distribution for Witherspoon Factor (N) is a special mixed-distribution that consists of an exponential distribution and a normal distribution (Figure 1). This distribution employs a working hypothesis for a statistical scaling factor between the dilation of a fracture (i.e., mechanical aperture) and the hydraulic aperture of a fracture (i.e., cubic-law effective mechanical aperture; Witherspoon et al., 1980). This scaling factor enables estimation of closed shear-fracture hydraulic aperture (positive compressive effective normal stress) with surface roughness, multi-stranding contact area, and aperture anisotropy taken into account via laboratory measurements combined with models (Li et al., 2021; Hyman et al., 2021; Welch, et al., 2022).

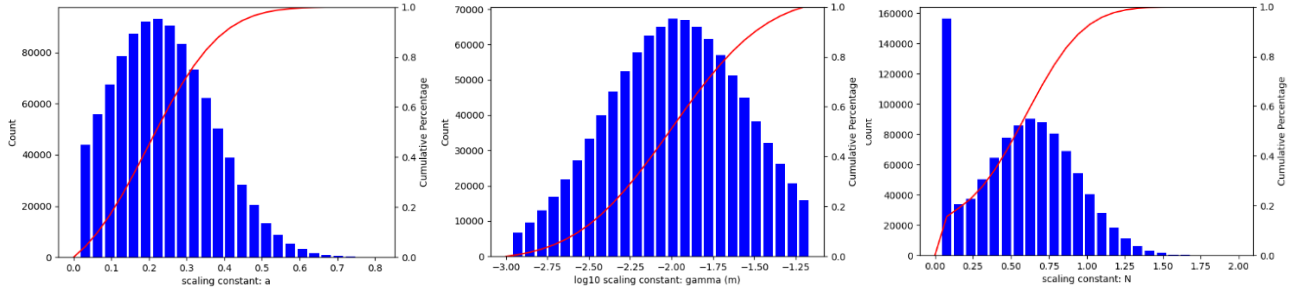


Figure 1: Distributions used in GeoDT including (left) truncated normal, (center) truncated log-normal, and (right) special. For more information about these distributions and associated parametrization refer to Frash et al., 2021.

Well layout and design are also among the randomly sampled parameters. To improve usefulness for the model, we require discoverable trends between natural fracture effects, stress effects, and well design options. Therefore, we developed a systematic structure to populate interrelated stochastic orientation parameters. As will be shown, this structure allows us to preserve the no site specific measurements premise of the base case while also providing a tool to identify key parameters that strongly influence EGS productivity.

First, the y-axis of the 3D domain is set as North and parallel to the minimum principal in-situ stress. The x-axis of the domain is set as the maximum horizontal principal stress direction and the z-axis is set as the vertical principal stress direction. Note that the principal stresses define these ordinates. The terms North, East, and vertical are used only to aid description of the geometry. Matrix rotations can be used to match our results to any orientation of actual subsurface stresses.

Second, we define a set of stochastic well geometry parameters (Figure 2). The production wells are placed relative to an injection well. The geometries that we consider are symmetric and follow the principle of fracture caging. However, this choice does not imply that we are assuming that fracture caging will occur. The orientation of the injection well is limited to dip directions and dip angles in the North-East lower-hemisphere quadrant (i.e., injection well azimuth of 0° North to 90° East and dip of 0° horizontal to 90° vertical). Due to Cauchy stress tensor symmetry, this orientation octant covers all possible angles between the well and the principal stresses.

Third, we define three natural fracture sets and we limit well orientations. Examples of triple conjugate joint sets are ubiquitous in nature, so we assume the same here. We take the dip direction as 90° clockwise from strike, viewed from above. To impose structure, we set the first joint set (Table 1) as sub-perpendicular to the injection well. This first set of fractures have a South-East strike and are steeply dipping from 67° to 113°, so most fractures in this set will be sub-perpendicular to the wells. Dip of greater than 90° captures fractures with strike +180°, in other words having North-West strike. The second fracture set is sub-vertical and sub-parallel to the wells. The third fracture set is sub-horizontal and sub-parallel to most wells. Note that the common reference here is with respect to the stress state, so the sub-parallel and sub-perpendicular fracture sets with respect to the well are not fully consistent.

Model outputs include: (1) a complete list of the randomly sampled input values, (2) electrical power production over time, (3) produced fluid enthalpy and temperature over time, (4) production mass and volume flow rates, (5) maximum generated earthquake magnitude, (6) total boundary leakage/inflow rates, (7) injection pressures, (8) natural fracture and hydraulic fracture stimulation counts, and (9) 3D visualization of the fracture and flow networks. In the next section, we present some example results from a set of 50,000 model runs. These 50,000 runs took 5.5 cpu days to complete on a desktop computer. Split between 6 threads the actual wall time was 1.8 days.

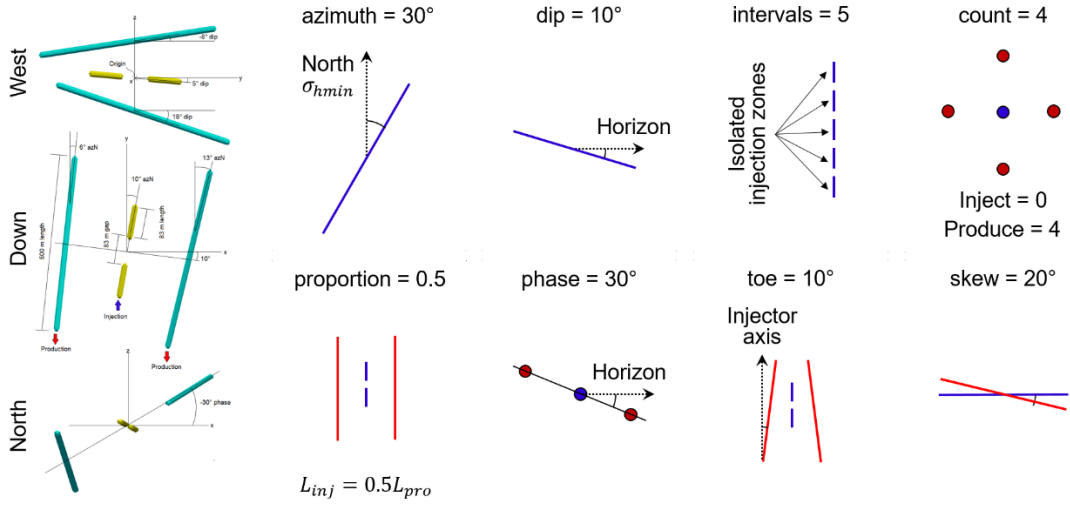


Figure 2: Structure for randomized well placement including injection well azimuth and dip, production well spacing and count, and 3D complexity via skew, toe, and phase. The injection well is broken into a number of zone-isolated intervals as could be implemented using packers or limited-entry casing perforations. The production wells could be longer or shorter than the injection well as defined by the proportion parameter. Other than the single production well scenario, all geometries are revolved-symmetric about the injection well and centered on coordinates of (0,0,0).

3. COMPILED RESULTS FOR BASE CASE WITH 50,000 SAMPLES

We will present results from this stochastic analysis in a sequential way that we hope will aid understanding. To begin, we will show the 3D fracture and flow network for a high-producing EGS system. After, we will show the 3D network for a low-producing EGS system. This establishes a basis on which we can then more closely investigate the statistics of the predictions and their implications.

3.1 Example high production scenario

Let us start our presentation of GeoDT results with a high-performance scenario that produces more than 22 MWe continuously over 20 years. In this example (Figures 3 and 4), the injection well is drilled at 26° azimuth and 6 ° dip (ref. min. principal stress) and is broken into 10 injection intervals. The target injection rate into each interval is 0.042 m³/s, giving a total realized injection rate of 0.42 m³/s.

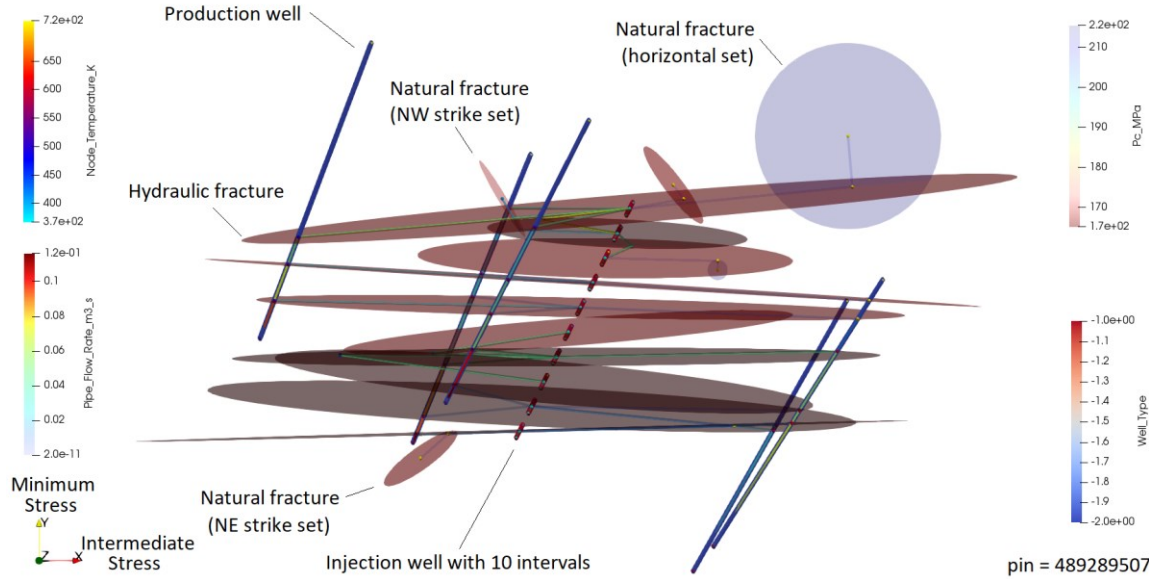


Figure 3: High-production 22 MWe scenario with 5 production wells, 10 injection intervals, and 767 m well spacing. To the North is an example of three injection intervals feeding into a single hydraulic fracture that ultimately produces from three production wells. Multiple production wells and injection intervals help to minimize thermal short-circuiting and to minimize fluid leakage out of the injection zone. Hydraulic fracture and shear fracture stimulation is predicted, not assumed. This is why different hydraulic fractures have different radii. Only fractures that connect to the flow network are shown, the figure would be too complicated otherwise.

The scenario shown here (Figures 3 and 4) holds many traits in common with other high-production examples. First, the bulk flow rate is quite high which causes the produced enthalpy to decline within even the first year of the project. However, this high flow rate combined with large heat transfer area across the fractures achieves sustained high energy-production rates. Second, the bottom-hole injection pressure (170 MPa) exceeds the minimum principal stress (165 MPa) continuously throughout the project. This causes fractures in the flowing network to be hydro-propelled (i.e., held open by positive net pressures) rather than propped by asperities or solid proppant particles. Third, the injection rate is evenly distributed among many injection intervals and many production wells. Increasing the number of wells and injection intervals lowers the likelihood that a single short-circuit will hinder long-term production. Fourth, the system relies heavily on hydraulic fractures rather than natural shear fractures. High-permeability natural fractures are excellent for reducing injection pressures, but finding them depends on luck. This is because we rarely, if ever, know where permeable natural fractures are located before drilling commences. Fifth, the distribution of flow through fractures is unequal. Even small differences in the hydraulic apertures of fracture segments (e.g., 0.1 mm) is sufficient to induce unequal flow that ultimately causes early thermal breakthrough. In the laboratory, we routinely observe fracture hydraulic aperture variabilities of >2.0 mm (Welch et al., 2022). Combined, the key message that this model tells us is: successful EGS requires the operator being able to force the rock into behaving the way we want it to. We require high surface area and high flow rates, even if the consequence is high injection pressures and a few more wells than the theoretical EGS minimum of two.

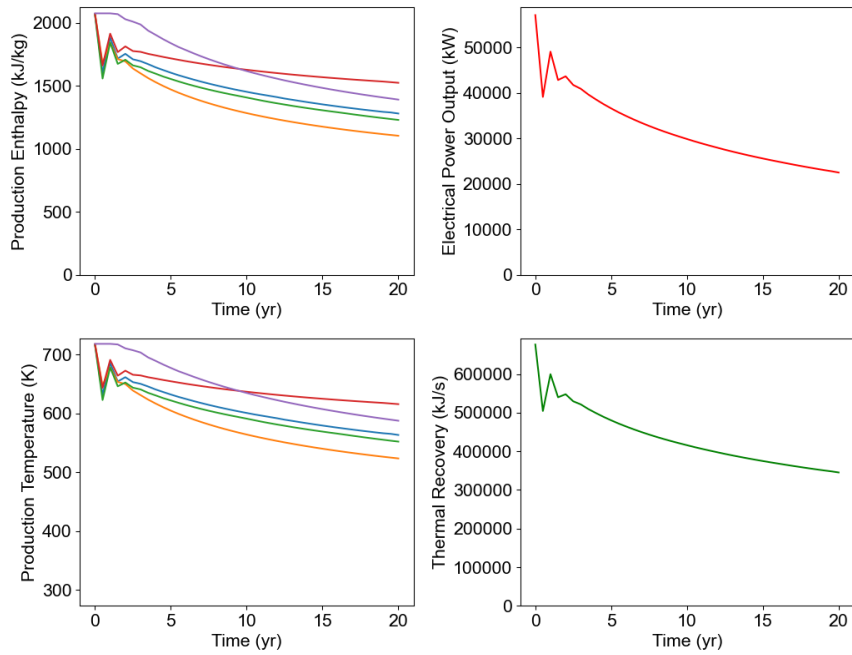


Figure 4: Time-series thermal and electrical power output predictions for the above 3D scenario. Different color lines signify different production wells. Early time oscillations are caused by the large 0.5 yr time-steps we used in GeoDT. All but one of the wells in this example experience thermal breakthrough within the first year. After 20 years, electrical power output of 22 MWe represents only 6.5% of the thermal power output of 340 MWt from this EGS system that uses the single-flash Rankine cycle. Our forthcoming analysis does not investigate the early power production that can exceed 50 MWe.

3.2 Example low production scenario

Understanding the design decisions that help make EGS successful also requires understanding about what can cause EGS to fail. This understanding helps to justify expensive decisions that increase the likelihood of moderate success over the pursuit of low-probability scenarios that could hypothetically be more productive and more economical. In effect, we need to appeal to the investment mentality and avoid the gambling mentality by carefully considering potential gains, potential losses, and probabilities.

Lacking site-specific data, the base case 50,000 models data provided many examples of failure (e.g., production of less than 0.1 MWe at 20 years). The majority of the failure scenarios involved drilling sub-parallel to the dominant fractures in the site. This situation hinders stimulation of fractures that hydraulically connect the injection wells to the production wells. In practice, this can occur as a consequence of not knowing the in-situ stress state, especially the direction of the minimum principal stress. However, this type of failure is relatively intuitive and it is rare to have no knowledge about the in-situ state of stress (e.g., World Stress Map, 2020).

We will focus on a failure scenario where the design was reasonable, but ultimately fails to perform (Figures 5 and 6). Our selected scenario uses wells drilled within 30° of the minimum principal stress direction (e.g., a case with ±30° uncertainty in minimum principal stress direction). This direction enables the injection well to connect to the production well via hydraulic fractures. Two wells are drilled to save on cost, but this choice means that less data is available to characterize the site. More crucially, this choice means a low probability of discovering hidden high-permeability natural fractures.

Lacking data to prove otherwise, our stochastically generated model scenario places an unknown high-permeability natural fracture sub-parallel to the injection well (green). This fracture is close to the injection well, but does not intersect it, making it invisible to most, if not all, site investigation techniques. The model then predicts that this sub-parallel horizontal fracture causes a short circuit between two injection intervals that then connect to the production well by only a single hydraulic fracture. The remaining three injection intervals experience a similar fate due to another sub-parallel northeast striking fracture. However, the hydraulic fracture that dominates these three southern injection intervals fails to connect to the single production well because the uncertainty in the minimum principal stress direction was underestimated in the design. Thus, out of five injection intervals, only two actually produce and the remainder leak away to locations where large damaging induced seismic events could be triggered. This situation produced a high risk if large induced seismic events and ultimately fails to produce much electrical energy, yielding a maximum of 500 kW and eventually 100 kW after 20 years of production.

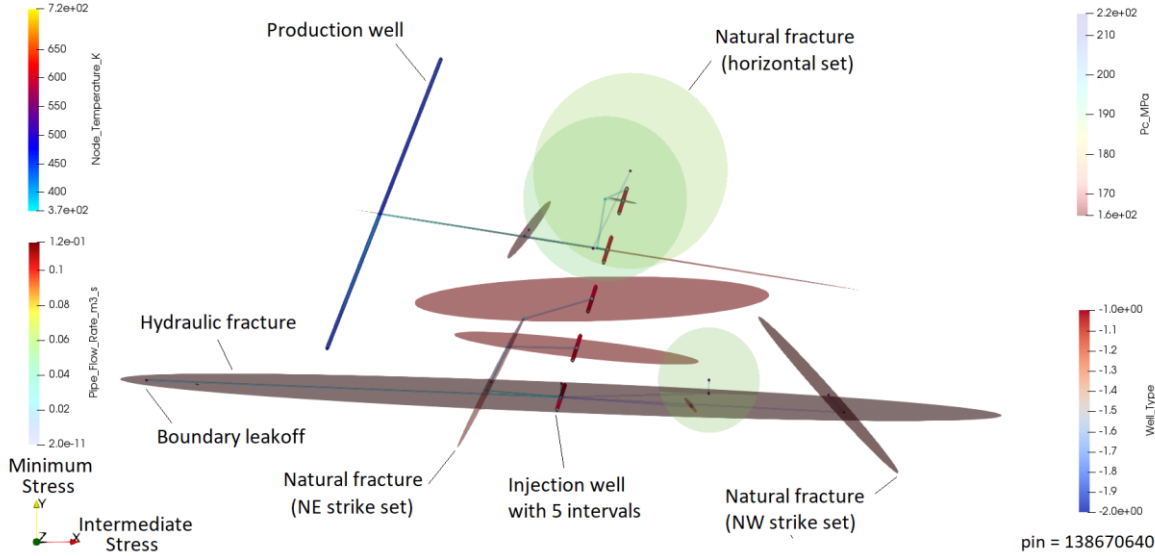


Figure 5: Low-production 0.1 MWe scenario with 1 production well, 5 injection intervals, and 800 m well spacing. Three of the five injection intervals fail to connect to the production well and instead leak off to the boundary. The remaining two injection intervals connect via undetectable pre-existing hydraulically conductive natural fractures causing a thermal short-circuit that limits heat transfer area. Furthermore, the uncased interval of the production well was too short, failing to account for uncertainty in the minimum principal stress direction.

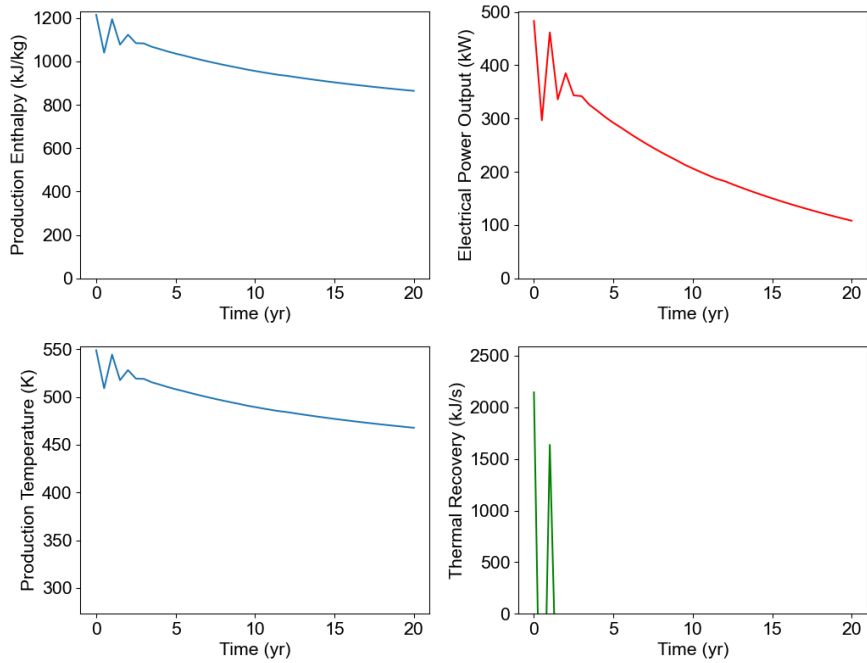


Figure 6: Time-series thermal and electrical power output predictions for the above low-performance scenario.

Looking closer, we can anticipate that microseismic monitoring would not guarantee diagnosis of this situation. For example, the southern hydraulic fracture would be tensile dominated, causing low microseismicity. Meanwhile, the northwest fracture cluster could be very noisy due to interaction with the natural fractures. To the observer, this would indicate dominant fracture stimulation to the northeast of the injection well and could lead to placement of the single production well in this area. Similarly misleading microseismic data has been observed and confirmed in laboratory block hydraulic fracture experiments (Frash et al., 2015). Unless zone-specific tracer studies were employed, it would be unknown that the southern hydraulic fracture missed the production well until it is too late to prevent damaging induced seismicity. This is an understandable, but unfortunate, scenario that could arise.

Many options are available to prevent the failure scenario shown here. First, the production well could have been longer to better account for uncertainty in the minimum principal stress direction. Second, the injection intervals could have been spaced further apart to reduce interactions via unknown natural fractures. Third, an additional production well could have been drilled to the southeast to intercept flow from that side of the injection well, effectively increasing the heat transfer area. Fourth, the production well spacing and the injection well flow rate could have been better optimized to make the most of this non-ideal situation.

3.3 Performance metrics by result categorization

Mining the results of this stochastic analysis can be accomplished using any of many methods, including black-box machine learning. However, we seek fundamental understanding that can help us to understand what is needed to optimize EGS designs and why. We chose to start this process by categorizing the results. Selected categories include: (A) fracture caged systems producing more than 5 MWe after 20 years; (B) very productive systems generating greater than 20 MWe after 20 years; (C) seismogenic systems at risk of maximum earthquake magnitudes exceeding 3.0 Mw; and (F) failed systems that produce less than 0.1 MWe after 20 years. Note that this electrical power production calculation uses the Single-flash Rankine Cycle which requires high enthalpy produced water to function and which does not account for more modern power generation technologies such as the binary cycle. Model outputs include fluid enthalpies and rates which provides the required inputs to evaluate the use of alternative power cycles for economic assessments.

Next, we created a normalized box-plot (Figure 7) of controllable input and output values separated by the categories (A to F). Plotted values are normalized to 0.0 for the minimum value in the entire data set and 1.0 for the maximum value. Percentages in the axis titles give the ratio of the 50,000 scenarios that meet the category requirements. From this plot we can identify correlations and trends. For example, increased reservoir depth (ResDepth) correlates with the high-producing categories A and B. However, ResDepth is weakly correlated with seismicity (C) and is not correlated with failure scenarios (F). Looking across the input variables and referencing Table 1, we can see the following predicted key relationships for high power output and fracture caging:

- Moderate reservoir depths (ResDepth): 7000 to 9400 m
- High thermal gradients (ResGradient): 45 to 55 °C/km
- Low stress anisotropy (Ks3): 0.6 to 0.9
- Moderate circulation injection rates (Qinj): 0.030 to 0.046 m³/s
- Higher well counts to ensure against leaks (w_count): 3 to 6 production wells
- Wells closer to parallel with the minimum principal stress (w_azimuth & w_dip): 0° to 45°
- A modest ratio of injection zone length to production well length (w_proportion): 0.56 to 0.88
- Maximized numbers of injection intervals/zones (w_intervals): >6 intervals
- Moderate well inner diameters (ra): 0.12 to 0.19 m (5.0 to 7.5 in)

Using these observations, we can now filter the results to only include the parameters in the bullet list above. However, the number of samples remaining in this filtered set is only 53 (0.11% of the results). Nevertheless, we can now crudely compare the ratio of successful scenarios between the full set where minimum principal stress direction is unknown to a set where it is known (Figure 8). This comparison shows a clear potential for optimization and motivates another 10,000 sample run of GeoDT using the refined input parameter space. The new model set confirms that the reduced parameter set (c.f., bullet list above) statistically increases EGS productivity (16% vs 2%).

3.4 Performance metrics by input parameter using the refined parameter set

We used the general statistics (Figure 8) to identify a more favorable parameter set for EGS power production. Next, we investigate the influence of individual parameters on EGS performance in the reduced parameter set. This investigation aims to identify design parameters that can be optimized within the reduced parameter set. It is important to note that this reduced parameter set is still broad compared to what detailed site data could achieve for a real site. To avoid excessive paper length, we chose not to investigate a specific site scenario where uncertainties in the input parameters could be reduced and the associated optimized parameters could be refined.

First, let us look at predicted power output as a function of reservoir depth (Figure 9). Here, the trends are weak with a slight increase in >20 MWe systems (blue) for the deeper reservoirs. However, the likelihood of a poor power production at <0.1 MWe (red) also increases with depth. Our subjective comparison of this behavior to the three-dimensional results suggests that flow tends to favor larger shear fractures (i.e., faults) at deeper depths because of increased stress anisotropy causing shear stimulation to become relatively easier than sustained hydraulic fracture stimulation. More shear fracture stimulation tends to associate with more diffusive flow (i.e., more leakoff) and a reduction in the number of production wells connected to each injection well interval.

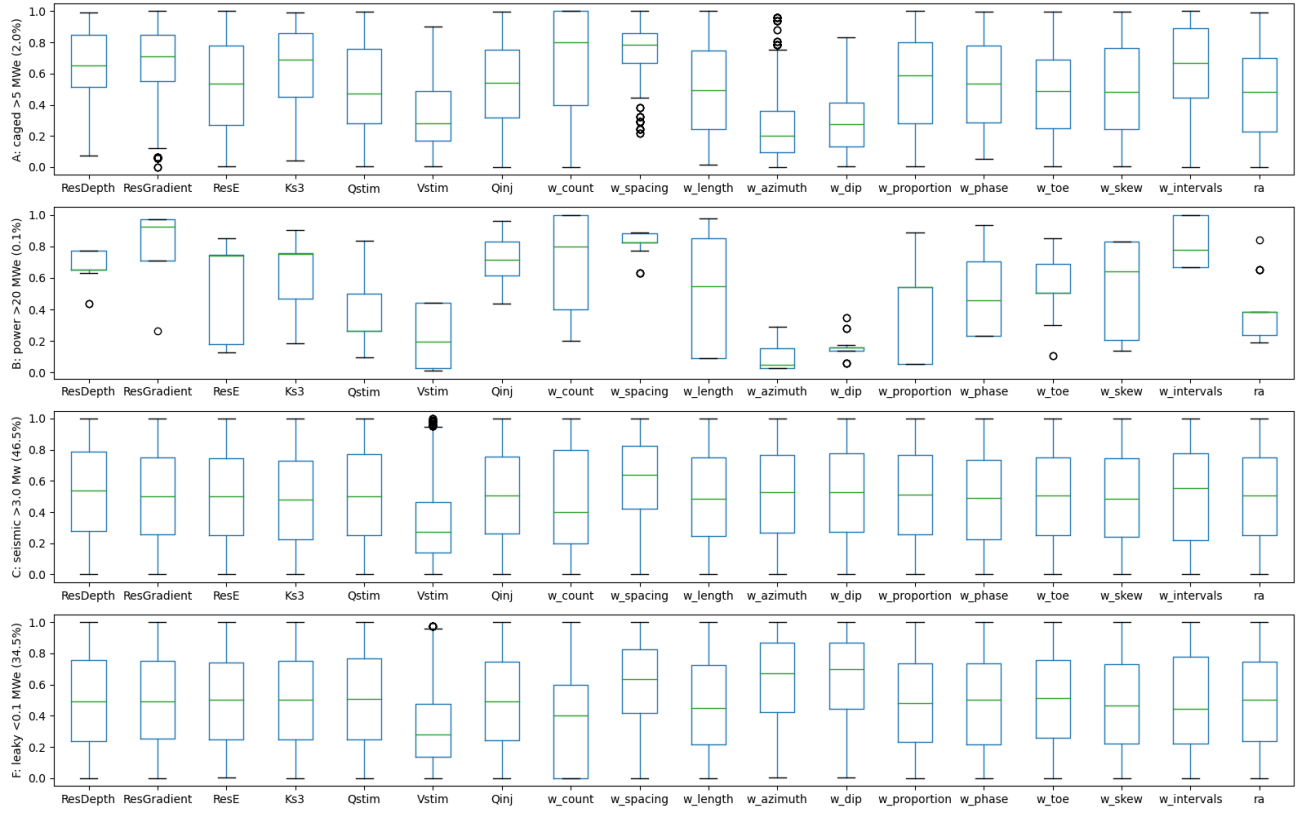


Figure 7: Normalized box plots for categorized scenarios (A, B, C, and F). Values are normalized by the minimum (0) to maximum (1) range of the input parameters. Differing trends for a parameter in opposing categories (e.g., A versus F) indicate the parameter is important to increase the probability of creating a successful EGS system. For example, the importance of drilling close to parallel to the minimum principal stress direction is evident by low values of well azimuth and dip associating with categories A and B (w_azimuth and w_dip). Percentages in the y-axis labels indicate the proportion of the 50,000 sample set that meet the criteria of each category (see Section 3.3). Parameter names are defined in Table 1.

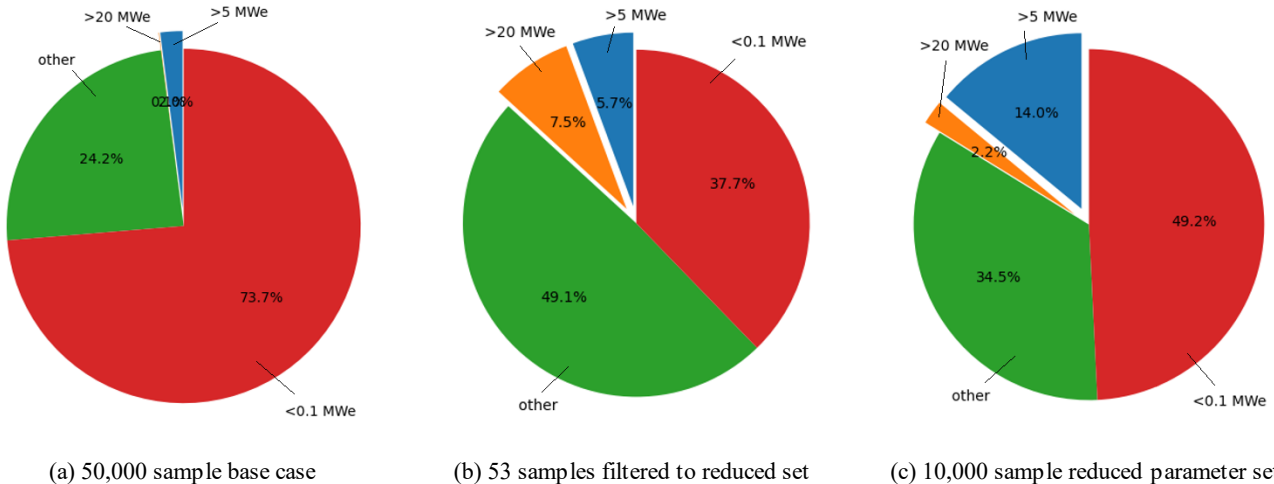


Figure 8: Ratios of productive EGS systems for (a) the base case with no site-specific data at 50,000 samples, (b) filtered results with a reduced range of input values yielding only 53 samples, and (c) revised predictions using reduced parameter ranges and 10,000 samples (c.f., bullet list above). Increased reservoir temperatures and drilling sub-parallel to the minimum principal stress are key factors for increasing the probability of a high-output EGS system (>5 MWe for 20 years).

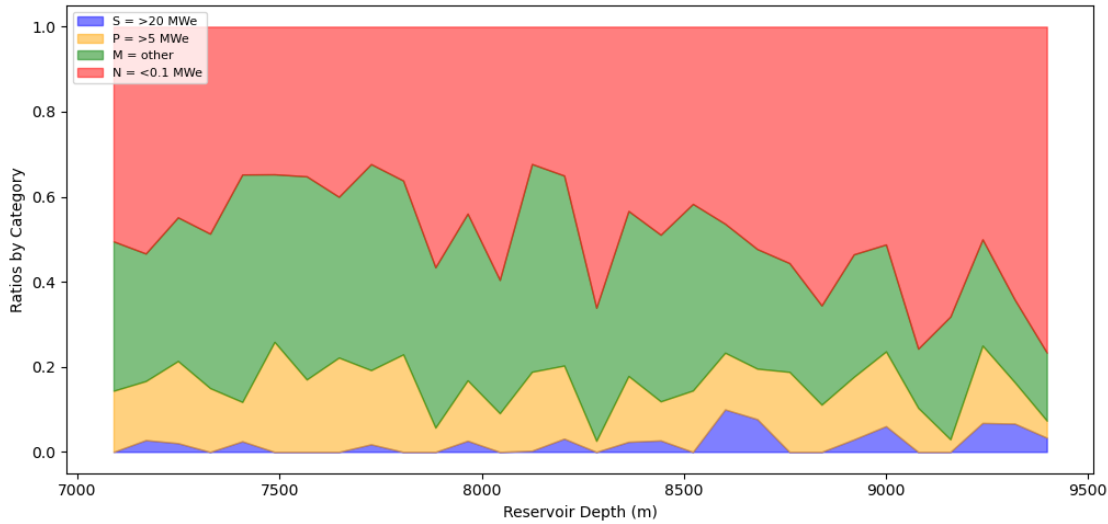


Figure 9: Power output as a function of reservoir depth showing no systematic optimizable trends.

Second, let us inspect predicted power output as a function of well spacing (Figure 10). Here, the trend is strong and shows optimal spacing within the range of 400 to 1100 m. It is also possible to claim that a better optimum could exist between 800 and 1000 m spacing, but we will later show that GeoDT predicts that this larger spacing brings a greater probability of damaging induced seismicity. Furthermore, it is important to point out that the probability of early thermal breakthrough can be reduced by optimizing the flow rates as a function of well spacing. However, the highest long-lived per-well outputs are only achievable at high flow rates (e.g., $> 0.03 \text{ m}^3/\text{s}$ per injection interval), which in turn require greater well spacing to provide ample heat exchange area. Our subjective interpretation of this result suggests that spacing closer than 400 m results with an increased risk of low energy production while a spacing greater than 1100 m tends to associate with a greater probability of flow leaking out of the site. However, we have not yet verified that this effect is not a consequence of our selected domain size at 3 km x 3 km x 3 km (i.e., $\pm 1.5 \text{ km}$ from (0,0,0)) which is constant for all these predictions.

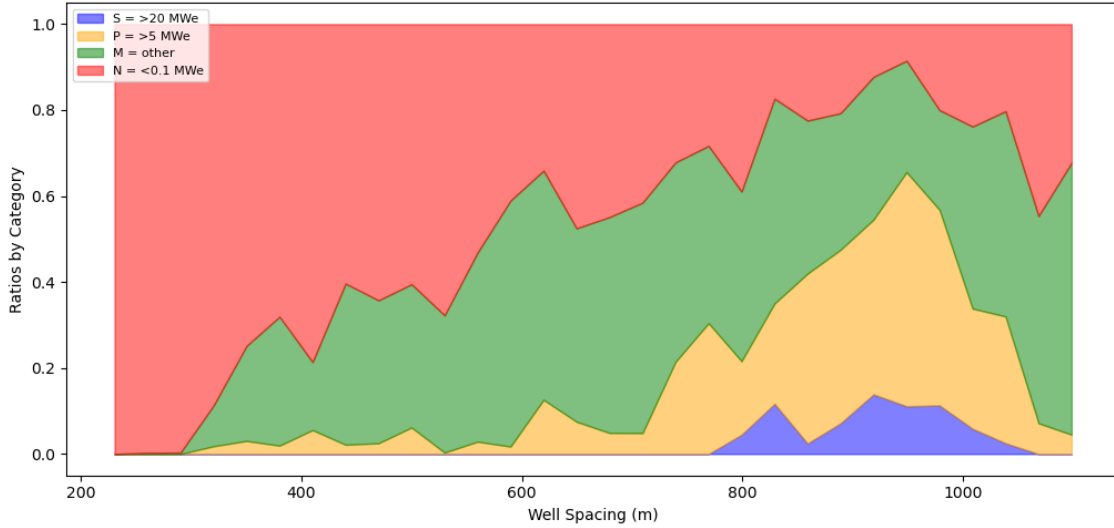


Figure 10: Power output as a function of well spacing showing optimal ranges of 400 to 1100 m or 800 to 1000 m, depending on perspective about seismic risk tolerance. We suggest an optimum of 400 to 700 m.

Third, we seek an optimization of the number of production wells and injection intervals (Figure 11). Economically, fewer wells is better for keeping the capital costs lower. However, more wells could be necessary to increase the likelihood that injected fluids will be contained within a target volume of rock to limit induced seismicity risk (i.e., fracture cage). Further, more wells could improve the sweep efficiency of fluid through the fractures to delay thermal breakthrough while increasing overall power output. Lacking a complete techno-economic analysis, we will inspect the benefits of more wells and more injection intervals separately from cost. These results predict that increasing well count can increase the probability generating $>5 \text{ MWe}$ for 20 years (e.g., 10% with 3 wells versus 22% with 6 wells). The star performers yielding $>20 \text{ MWe}$ for 20 years peak at 4 production wells. Therefore, we anticipate that 3 to 4 production wells could be sufficient for achieving high power output at a relatively low capital cost if the other parameters of the design are adequately optimized.

The effect of increasing the number of injection intervals is unclear in the reduced parameter set. From inspection of the three-dimensional results (e.g., Figures 3 to 6), the predictions indicate that larger numbers of injection intervals can prevent thermal short-circuits (i.e., premature cooling of the production wells). However, the spacing of these intervals is also relevant because too close of spacing counters the gains from an increased number of intervals. Our expectation is that a maximum number of injection intervals will be optimal because it will offer versatility in site control and adaptability to changing ground conditions over time. If this expectation is correct, downhole tool technology is the limitation because simultaneous isolation and specification of flow rates across even two isolated zones will be a challenge with currently available tools. Instead, we may need to rely on limited-entry systems where flow rates into different intervals of the well is limited by casing perforation diameter instead of fracture permeability. This option offers benefits for flow control, but comes at the price of demanding very high injection pressures.

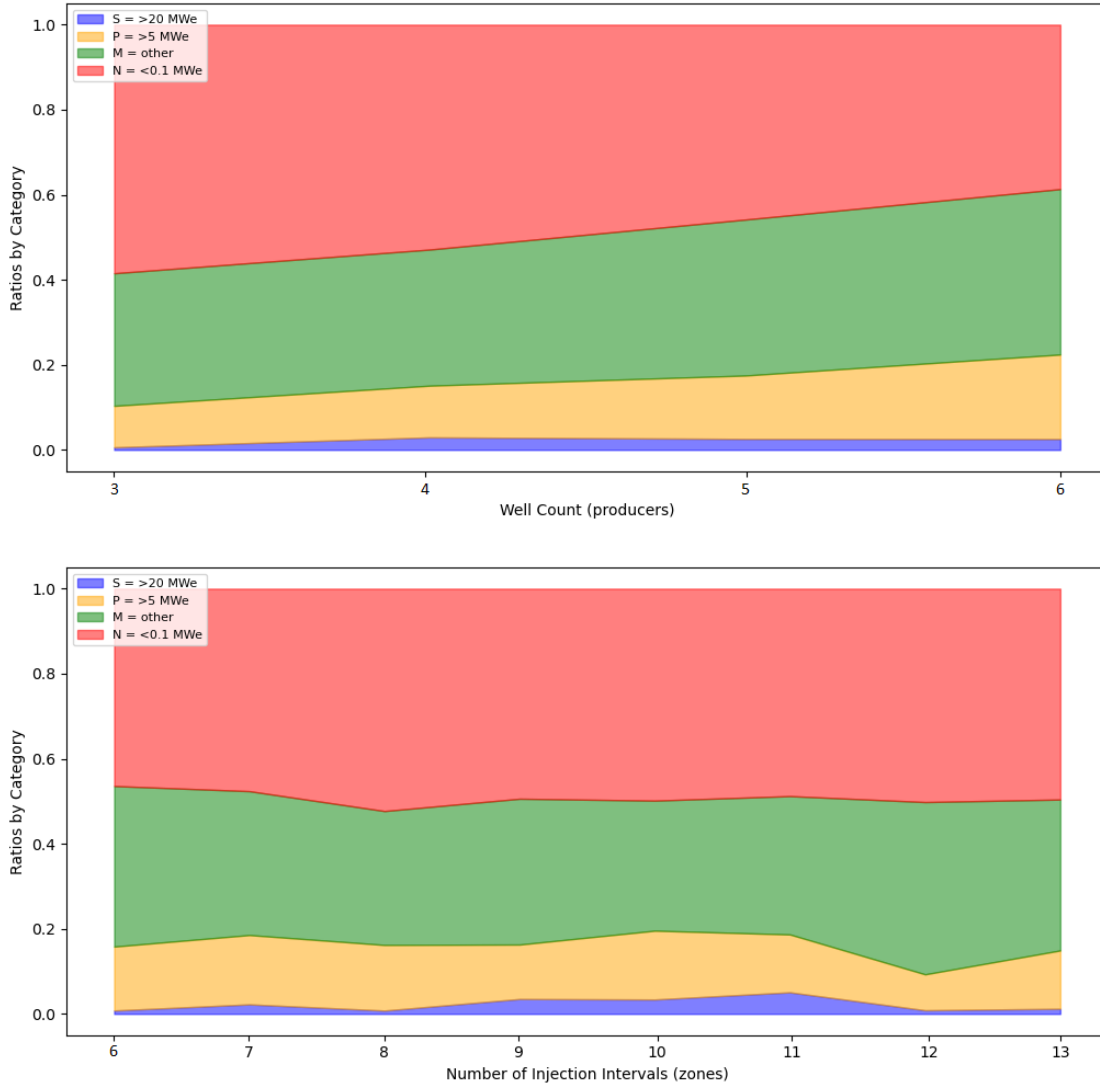


Figure 11: Power output as a function of number of production wells and number of injection intervals showing a trend of increasing output with larger well counts and an unclear trend with larger numbers of injection intervals.

Lastly, we seek control over maximum induced seismic magnitudes. GeoDT includes prediction of maximum seismic magnitudes using its power-law scaling functions. The relationship is based on Gutenberg-Richter law (Richter and Gutenberg, 1956) and rupture-area moment-magnitude (M_0) calculations (Frash et al., 2021). While imperfect, this approach enables preliminary estimation of the impact of well spacing on induced seismic magnitudes (Figure 12). Based on our results, the probability of a maximum 3.0 Mw induced seismic event first exceeds 50% at a well spacing of 720 m. However, it is not yet known if this estimation is overly conservative or overly risky. This uncertainty stems from a lack empirical field-scale evidence to validate fracture caging and the simplified physics employed by GeoDT. Therefore, we tentatively suggest a maximum well spacing of 700 m to limit seismicity to unfelt seismic events (e.g., <3.0 Mw).

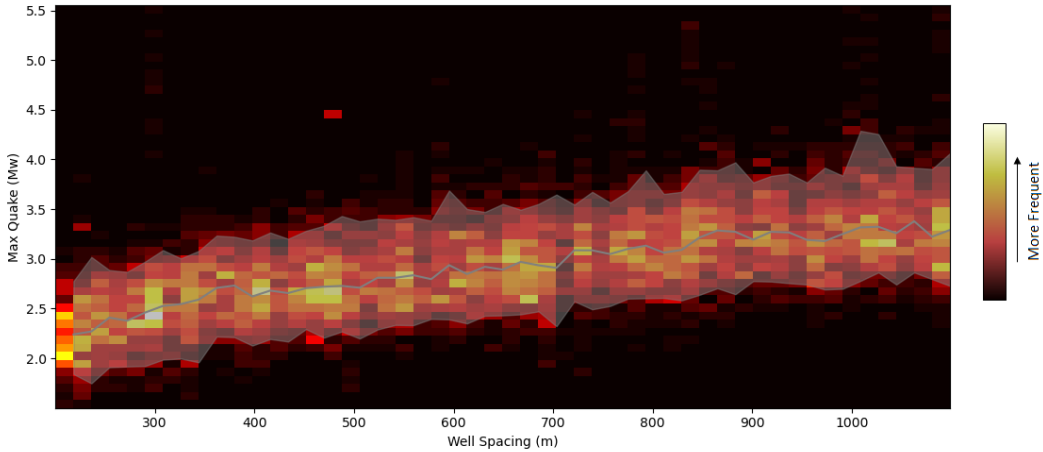


Figure 12: Maximum seismic event magnitudes versus well spacing as predicted by GeoDT for the reduced parameter set. This plot shows a 2D histogram with hotter colors indicating more occurrences within the 10,000 sample scenarios. The 90% confidence interval and sample mode of the data are plotted in grey.

4. DISCUSSION

The model results and analysis presented thus far represent a single iteration of what can be done to identify optimized EGS designs. With more site data and more iterations we anticipate that this approach could be used to identify site-specific optimized well layouts and designs. In this process, tools such as GeoDT offer a quantitative-probability approach to justify down selection of site development plans that can then be evaluated using detailed high-fidelity models or selected for implementation. Our future plans for GeoDT include adding more power-cycle options and adding tools to estimate well and surface infrastructure costs so that economically optimized designs can be rapidly identified. Furthermore, we seek to identify site-specific well control options that would maximize power output by optimizing the flow rates and pressures for each well.

To increase the probability of creating high-producing EGS (>20 MWe for >20 years) and to decrease the probability of creating low-producing EGS (< 0.1 MWe), our analysis points to several key technologies and design features:

1. Drilling the injection well(s) close to parallel to the minimum principal stress direction is crucial for increasing the likelihood that a connected injector-producer system is created.
2. Deeper wells and higher temperature gradients could be beneficial for increasing EGS power output, but this is dependent on the ability to create and sustain open-permeable fractures. A key technology to ensure success at deeper depths is sustained high-rate high-pressure pumping for the life of the project.
3. To reliably contain injected fluids and to minimize the risk of large induced seismic events, two or more production wells should be drilled around the injection well. A key technology here is fracture caging to prevent uncontrolled fracture stimulation.
4. Increased EGS power output requires controlled flow into multiple fractures to maximize active heat exchange area. High-pressure zonal isolation technology is key to this success, with limited entry stimulation providing one option.
5. All site measurements will have uncertainty and hidden permeable natural fractures can be present unless it is proven otherwise. Well placement could help compensate for this uncertainty by using longer open-hole or screened production wells and by using geometric tricks such as skew (Figure 2).
6. Subsurface uncertainty dominates fracture locations and properties. Robust designs should consider both the knowns and the unknowns to identify successful designs that perform well in as many scenarios as possible. The most robust designs that we identified all included three or more production wells, and six or more isolated injection intervals.
7. Boundary conditions (e.g., well pressures and flow rates) can be manipulated to get the most out of an EGS (Frash, 2021). This is effective on a site-specific basis using per-well per-interval measurements and rapidly updated forward models.

5. CONCLUSIONS

In this paper, we presented a single iteration of design optimization for full-scale EGS using our open-source code GeoDT. A total of 60,000 predictive scenarios were modeled in 3 days of wall time using a standard desktop computer. The simulations included natural fracture parameterization and well placement, fracture hydraulic stimulation, network flow and pressure calculations, thermal production prediction for 20 years, and electrical power output prediction. In our runs, GeoDT sacrifices some accuracy to rapidly analyze numerous scenarios. Our results and analysis indicate that key factors to improve EGS productivity are: (1) drilling wells within 45° from the minimum principal stress direction, (2) drilling two or more production wells in the form of a fracture cage, (3) employing zonal isolation technology to combat short-circuiting risk, and (4) long-term high-pressure high-rate pumping for the life of the project. The results indicate that an optimal spacing between the injection and production wells for EGS could be from 400 m to 700 m. The lower limit of 400 m helps to avoid premature cooling of the production well. The upper limit of 700 m helps to protect against seismic events greater than 3.0 Mw. The presented results are intended to apply to all geologies by using multi-scale inclusive rock properties. The same model can be applied in site-specific contexts where uncertainty can be reduced. This work presents a base case where site data is lacking so that the value of reduced uncertainty can be assessed with respect to statistically improved site development plans.

ACKNOWLEDGEMENTS

This work is supported by Department of Energy (DOE) Basic Energy Sciences under FWP LANLE3W1. Additional support was provided by the Los Alamos National Laboratory's Laboratory Directed Research and Development – Exploratory Research program (LDRD-ER-20220175ER). We are grateful for this funding provided by DOE and LANL.

The Python code for this work was developed using components from the “Fat Crayon Toolkit” (Singh et al., 2019) and was inspired by the EGS Collab Project (DOE-GTO). We gratefully acknowledge all the contributors to the Fat Crayon Toolkit, especially its lead developer Joseph P. Morris.

We also gratefully acknowledge useful feedback from J. William Carey, Meng Meng, and Wenfeng Li during discussions concerning the development of GeoDT.

REFERENCES

Asadi, I., Shafiq, P., Hassan, Z.F.B.A, and Mahyuddin, N.B.: Thermal conductivity of concrete - a review, *Journal of Building Engineering*, (2018).

Bearsdmore, G.R. and Cull, J.P.: *Crustal Heat Flow*, Cambridge University Press, (2001).

Carmichael, R.: *Revival: Handbook of physical properties of rocks*, CRC Revivals, (1982).

Cooper, J.R. and Dooley, R.B.: Revised release on the IAPWS industrial formulation 1997 for the thermodynamic properties of water and steam, *The International Association for the Properties of Water and Steam*, (2007).

Frash, L.P.: GeoDesignTool/GeoDT, <https://github.com/GeoDesignTool/GeoDT>.

Frash, L.P.: Geothermal Design Tool (GeoDT), *Proceedings, 46th Workshop on Geothermal Reservoir Engineering*, Stanford University, Stanford, CA (2021).

Frash, L.P., Fu, P., Morris, J., Gutierrez, M., Neupane, G., Hampton, J., Welch, N.J., Carey, J.W., and Kneafsey, T.: Fracture caging to limit induced seismicity, *Geophysical Research Letters*, e202GL090648, (2020).

Frash, L.P., Gutierrez, M., Hampton, J., and Hood, J.: Laboratory simulation of binary and triple well EGS in large granite blocks using AE events for drilling guidance. *Geothermics*, (2015).

Frash, L.P., Welch, N.J., Meng, M., Li, W., and Carey, J.W.: A Scaling Relationship for Fracture Permeability after Slip, *Proceedings, 55th US Rock Mechanics/Geomechanics Symposium*, Houston, TX, (2021).

Gutenberg, B. and Richter, C.F.: Magnitude and Frequency of Earthquakes, *Annali di Geofisica*, (1956).

Hamm, S., Hass, E., Winick, J., Tasca, C., Albayrak, F., Augustine, C., Boyd, L., Eugeni, E., Thomas, H., Reinhardt, T., Richard, C., Segneri, B., Snyder, N., Wall, A., and Williams, T.: *GeoVision: Harnessing the heat beneath our feet*. US Department of Energy, (2019).

Huber, M.L., Perkins, R.A., Laecke, A., and Friend, D.G.: New international formulation for the viscosity of H₂O, *Journal of Physical and Chemical Reference Data*, (2009).

Hyman, J.D., Sweeney, M.R., Frash, L.P., Carey, J.W., and Viswanathan, H.S.: Scale-Bridging in Three-Dimensional Fracture Networks: Characterizing the Effects of Variable Fracture Apertures on Network-Scale Flow Channelization, *Geophysical Research Letters*, (2021).

Jeppson, R.W.: *Steady Flow Analysis of Pipe Networks: an Instructional Manual*, Reports, 300, (1974).

Kodur, V.: Properties of concrete at elevated temperatures, *International Scholarly Research Notices*, (2014).

Kosky, P., Balmer, R., Keat, W., and Wise, G.: *Exploring Engineering*. Elsevier, (2013).

Li, W., Frash, L.P., Welch, N.J., Carey, J.W., Meng, M., and Wigand, M.: Stress-dependent fracture permeability measurements and implications for shale gas production, *Fuel*, (2021).

Savitski, A.A. and Detournay, E.: Propagation of a penny-shaped fluid-driven fracture in an impermeable rock: asymptotic solutions. *International Journal of Solids and Structures* (2002).

Singh, A., Neupane, G., Dobson, P., Zoback, M., Morris, J., Fu, P., et al.: Slip tendency analysis of fracture networks to determine suitability of candidate testbeds for EGS Collab hydroshear experiment, *Idaho National Laboratory*, (2019).

Tester, J.W., Anderson, B.J., Batchelor, A.S., Blackwell, D.D., DiPippo, R., Drake, E.M., Garnish, J.D., Livesay, B., Moore, M.C., Nochols, K., Petty, S., Toksoez, M.N., and Veatch, R.W.J.: The Future of Geothermal Energy: Impact of Enhanced Geothermal Systems (EGS) on the United States in the 21st Century, *Massachusetts Institute of Technology*, Idaho Falls, ID, (2006), pp. 372.

Vitaller, A.V., Angst, U.M., and Elsener, B.: Laboratory tests simulating corrosion in geothermal power plants: influence of service conditions, (2020).

Waples, D.W. and Waples, J.S.: A review and evaluation of specific heat capacities, *Natural Resources Research* (2004).

Welch, N.J., Carey, J.W., Frash, L.P., Hyman, J.D., Hicks, W., Meng, M., Li, W., and Menefee, A.H.: Effect of Shear Displacement and Stress Changes on Fracture Hydraulic Aperture and Flow Anisotropy, Transport in Porous Media, (2022).

Witherspoon, P.A., Wang, J.S., Iwai, K., and Gale, J.E.: Validity of cubic law for fluid flow in a deformable rock fracture. Water Resources Research, (1980).

World Stress Map: <http://www.world-stress-map.org/>, (2020).

Zoback, M.D.: Reservoir Geomechanics, Cambridge University Press, (2018).